Spin-Crossover Nanocrystals

DOI: 10.1002/anie.200801673

Spin-Crossover Nanocrystals with Magnetic, Optical, and Structural Bistability Near Room Temperature**

Ishtvan Boldog, Ana B. Gaspar, Víctor Martínez, Pablo Pardo-Ibañez, Vadim Ksenofontov, Ashis Bhattacharjee, Philipp Gütlich, and José A. Real**

Dedicated to Professor Jan Reedijk on the occasion of his 65th birthday

Functional molecular materials with switching properties and memory transduction are of considerable interest in view of their potential technological applications.[1] Rational control of the growth of these materials on a nanometric scale is required, however, if they are to be successfully integrated into functional devices.[2] The miniaturization of functional molecular materials and the study of their chemical and physical properties on this scale is a subject of intense research activity in materials science.[3–5]

Spin-crossover (SCO) compounds are functional molecular materials which possess labile electronic configurations that are switchable between the high-spin (HS) and low-spin (LS) states in response to external stimuli (temperature, pressure, or light).[6] SCO compounds reveal differences in magnetism, optical properties, dielectric constant, color, and structure in the HS and LS states. These physical properties may change drastically in a narrow range of temperature and/or pressure, and even under irradiation at different wavelengths, for cooperative transitions exhibiting hysteretic behavior.[7,8] These characteristics have made the SCO phenomenon one of the most interesting examples of bistability in molecular materials. Many publications have underlined the potential applications of iron(II) SCO materials as sensors or memory devices.[9] Nanostructuration using the bottom-up synthetic approach is a fundamental requisite to achieve this goal.[2] At this point, it should be stressed that a reduction of the film thickness or particle size of an SCO material could affect its physical properties drastically since electronic bistability depends on the collective behavior of the SCO centers in the lattice. This cooperative mechanism, which is responsible for the occurrence of first-order phase transitions, is crucial for signal and memory generation. Determination of the critical particle size or film thickness that allows the hysteretic behavior to be conserved is therefore an essential aspect of this research.

Bottom-up nanostructuration has been successfully applied to the 3D SCO polymer $[Fe(pz)Pt(CN)_4]$ (**1**)[10] by layer-by-layer (LbL) epitaxial growth on gold surfaces. The resulting films,[11a,b] which have a thickness of approximately 150 nm, display similar spin crossover to that observed in the "bulk" material. Compound **1** exhibits a sharp first-order spin transition at room temperature with a hysteresis loop 25 K wide.[10b] This spin transition is accompanied by an easily detectable change of color between yellow-orange (HS) and deep-red (LS).[10] In addition, the spin states can be switched by irradiation with a red light pulse within the thermal hysteresis loop.[11b]

Water-in-oil microemulsions, also known as reverse micelles, have recently been applied to the synthesis of nanoparticles of the 1D iron(II) SCO polymer $[Fe(Htrz)_2(trz)](BF_4)$ (Htrz = 1,3,4-1*H*-triazole). The resulting surfactant-coated nanoparticles, which have an average size of less than 20 nm, display a spin transition with thermal hysteresis above room temperature similar to that reported for the "bulk" material.[12a] Previous studies on nanoparticles of this polymer demonstrated suppression of the first-order phase transition in favor of a continuous spin transition for particles of reduced size.[12b,c]

Herein we report the successful application of the bottom-up approach for the synthesis of surfactant-free nanometer-sized crystals of $[Fe(pz)Pt(CN)_4]$ (**2** and **3**) that display size-dependent magnetic and optical properties. The average size found for nanocrystals of $\mathbf{2}\cdot H_2O$ and $\mathbf{3}\cdot 2.5\,H_2O$ is $230\times230\times55$ and $61\times61\times21$ nm, respectively.

The syntheses were performed by mixing sodium bis(2-ethylhexyl)sulfosuccinate (NaAOT) stabilized water-in-oil microemulsions containing $Fe(BF_4)_2$, pyrazine, and $K_2[Pt(CN)_4]$ at constant W ($[H_2O]/[NaAOT]$; see Experimental Section for details). A distinctive color change from

[*] Dr. I. Boldog, Dr. A. B. Gaspar, V. Martínez, Prof. J. A. Real
Institut de Ciència Molecular
Departament de Química Inorgànica
Universitat de València
Edifici d'Instituts de Paterna
Apartat de Correus 22085, 46071 València (Spain)
Fax: (+34) 96-3544-855
E-mail: ana.b.gaspar@uv.es
jose.a.real@uv.es
P. Pardo-Ibañez
Institut de Ciència dels Materials
Universitat de València
Edifici d'Instituts de Paterna
Apartat de Correus 22085, 46071 València (Spain)
Dr. V. Ksenofontov, Dr. A. Bhattacharjee, Prof. P. Gütlich
Institut für Anorganische und Analytische Chemie
Johannes-Gutenberg-Universität
Staudinger-Weg 9, 55099 Mainz (Germany)

[**] Financial support from the Spanish Ministerio de Educación y Ciencia (MEC) (CTQ 2007-64727-FEDER), the Generalitat Valenciana (ACOMP07/110), and the European Network of excellence MAGMANET (contract: NMP3-CT-2005-515767-2) is acknowledged. A.B.G. thanks the Spanish MEC for a research contract (Programa Ramón y Cajal).

Supporting information for this article is available on the WWW under http://dx.doi.org/10.1002/anie.200801673.

light yellow to orange was observed after a few minutes along with the formation of a fine precipitate of coagulated nanocrystals. Syntheses at $W = 5$ with $C_{Fe^{2+}} = C_{Pt(CN)_4^{2-}} =$ 0.05 and 0.1 M yielded **2**·H_2O and **3**·2.5 H_2O, respectively, as orange-yellow solids after work-up. The growth of the nanocrystals takes place via content exchange between microdroplets of the microemulsion,[13] and their precipitation occurs at some particle size limit, apparently because of destabilization of the micelle. Preliminary experiments demonstrated that the size of the particles formed increases with W in the range $W = 5$–15, reaching a micrometer scale at $W =$ 15. In contrast, the particle size decreases as the concentration of the reactants in the aqueous phase increases.

The water content of **2**·H_2O and **3**·2.5 H_2O was established by thermogravimetric analysis. Water loss occurs in the interval 323–398 K, while complete water loss for the "bulk" sample occurs at around 443 K. Decomposition of these samples occurs at approximately 500 K. The FT-IR spectra of the isolated precipitates contain no characteristic bands for the AOT^- ion, thus proving the absence of a coating surfactant layer (see the Supporting Information). These spectra are practically identical to that of **1**·H_2O.

Figures 1a and 1b show TEM images of **2**·H_2O and **3**·2.5 H_2O nanoparticles dispersed in methanol and deposited on a TEM grid. The nanoparticles of **2**·H_2O are well-defined and are fairly monodisperse, with distinctive square faces with a side length of (230 ± 31) nm. The preferred orientation of the crystals parallel to the grid surface made their height determination by TEM difficult, therefore SEM images (Figure 1c) were taken. These images gave an estimated height of (55 ± 14) nm, which was also confirmed by AFM spot sampling (see the Supporting Information).

Complex **3**·2.5 H_2O consists of smaller nanocrystals with a morphology similar to that of **2**·H_2O. The average side length and height estimated from TEM images were found to be (61 ± 10) and (20 ± 5) nm, respectively. Analysis of the corresponding SEM images gave an estimated height of (27 ± 5) nm, which is in accordance with the value obtained by AFM spot sampling (see the Supporting Information). However, the quality of the nanocrystals is inferior and the height distribution is broader than for **2**·H_2O. This quality deterioration probably takes place beacuse of the lower stability of the $K_2[Pt(CN)_4]$ microemulsion at such concentrations, which sets a limit to the particle-size reduction upon increasing the concentration of salts in the aqueous phase. Nevertheless, the narrow distribution of the nanocrystals side length, especially for **2**·H_2O, is a significant finding given that deterioration of the nanocrystal quality and a broad distribution of their geometrical parameters are usually observed for large particles since multiple growth mechanisms could occur simultaneously.[2,3b] The TEM observations confirmed that the nanocrystal morphology remained unchanged after dehydration.

The powder X-ray diffraction patterns (XRPD) of the dehydrated nanocrystals collected at 293 K match that simulated for the HS structure of **1**·2 H_2O at 293 K (Figure 2).[10a] Integral width (β_{int}) values for the 011 and 022 reflections were used to determine the particle size based on Scherrer's equation,[2] with values of 156 and 83 nm being obtained for **2** and **3**, respectively (see the Supporting Information). As expected, the estimated particle size for **2** based on Scherrer's law is smaller than that obtained by TEM, whereas the opposite situation is true for **3**. This fact could, in

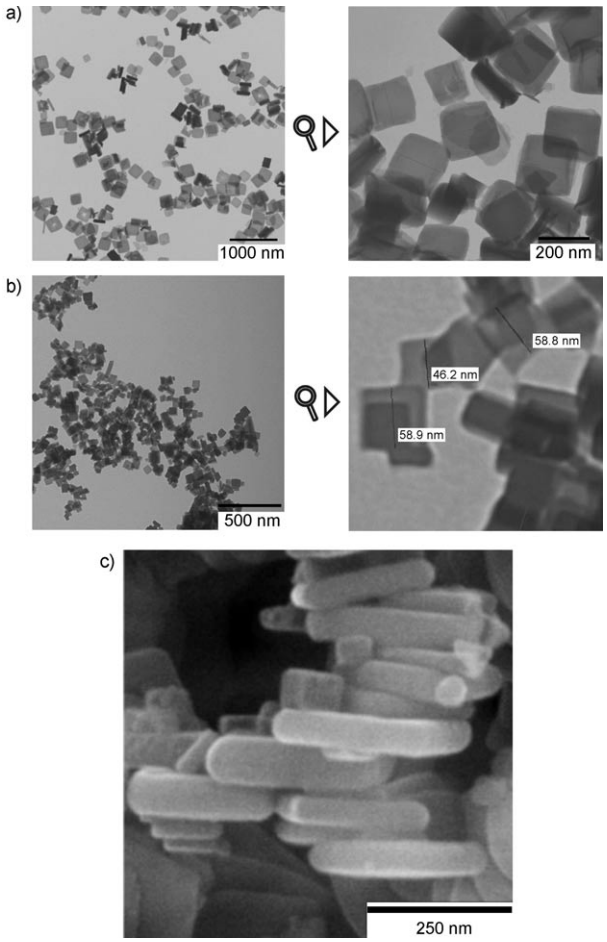

Figure 1. TEM images of **2**·H_2O (a) and **3**·2.5 H_2O (b). SEM image of **2**·H_2O (c).

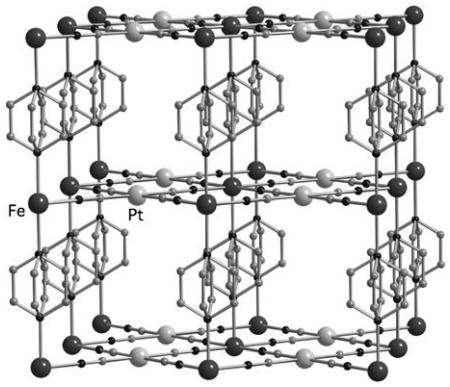

Figure 2. 3D porous framework of [Fe(pz)Pt(CN)$_4$]·2 H_2O (**1**·2 H_2O) showing the $\{Fe[Pt(CN)_4]\}_\infty$ sheets (002 plane) connected by pyrazine bridges rotationally disordered around the C_4 axis. Water molecules have been omitted for clarity.

principle, be partially due to an increase of the strain contribution to the profile broadening, which leads to an underestimation of crystallite size by the Scherrer equation for this system.

As in the bulk form,[10,11c] the magnetic properties of the nanocrystals depend strongly on the water content. For the sake of generality, the anhydrous form of these nanocrystals is considered the most important for primary characterization. Compounds **2** and **3** were obtained by heating **2**·H_2O and **3**·2.5H_2O, respectively, at 413 K for 2 h (see the Supporting Information). The thermal dependence of $\chi_M T$ for **1**–**3**, where χ_M is the molar magnetic susceptibility, is shown in Figure 3. At 300 K, $\chi_M T$ is equal to

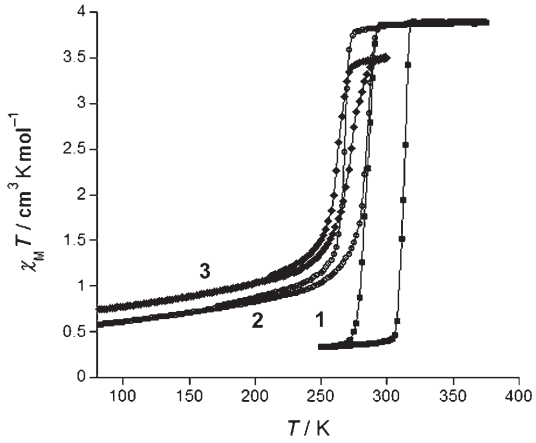

Figure 3. Magnetic properties in the form of $\chi_M T$ vs T plots for **1** (filled squares), **2** (open circles), and **3** (filled rhombuses) recorded in the temperature interval 2–350 K at a cooling/heating rate of 2 K min^{-1}.

3.85 cm^3 K mol^{-1} for **1**, 3.85 cm^3 K mol^{-1} for **2**, and 3.49 cm^3 K mol^{-1} for **3**. These values fall into the range expected for an Fe^{II} ion in the HS state, although the $\chi_M T$ value for **3** is lower due to a LS fraction at this temperature. On lowering the temperature, **2** and **3** undergo a similar SCO as that observed for **1**, although their characteristic critical temperatures are shifted downwards ($T_c^{\downarrow} = 266$ (**2**) and 265 K (**3**)). At 80 K, the $\chi_M T$ values of 0.62 (**2**) and 0.74 cm^3 K mol^{-1} (**3**) suggest a small residual HS fraction at low temperature, which agrees with the Mössbauer spectra. In the warming mode, $\chi_M T$ remains practically constant until the vicinity of $T_c^{\uparrow}$ (288 and 275 K for **2** and **3**, respectively).

The ^{57}Fe Mössbauer spectra of **2** and **3** recorded at two representative temperatures are shown in Figure 4. The characteristic isomer shift (δ, relative to α-iron) and quadrupole splitting (ΔE_Q) parameters, together with the percentage of the population in HS and LS states deduced from a routine least-squares-fit analysis of the spectra, are given as Supporting Information. The high-temperature Mössbauer spectra for both compounds show two different doublets, namely HS(1) and HS(2), which are characterized by δ values in the range 1.06–1.22 mm s^{-1} and quite different ΔE_Q values. For example, ΔE_Q for **2** is equal to 1.16(1) and 2.86(9) mm s^{-1} for the HS(1) and HS(2) doublets, respectively, at 295 K and the relative population of HS(1) is 88% while it is only 12% for HS(2). The intensity of the former doublet decreases upon cooling to 85 K and a new LS doublet grows ($\delta = 0.46(1)$ mm s^{-1}; $\Delta E_Q = 0.34(1)$ mm s^{-1}), whereas the population of the HS(2) doublet is practically temperature-independent. The population of the LS doublet at 85 K, where no further spin transition occurs, is around 88%. Similar δ and ΔE_Q values were found for **3**, where all the HS(1) sites also transform into LS sites at low temperature. The Mössbauer parameters of **1** compare well with those found for the Fe(1) site in **2** and **3** in the HS and LS states.[10b]

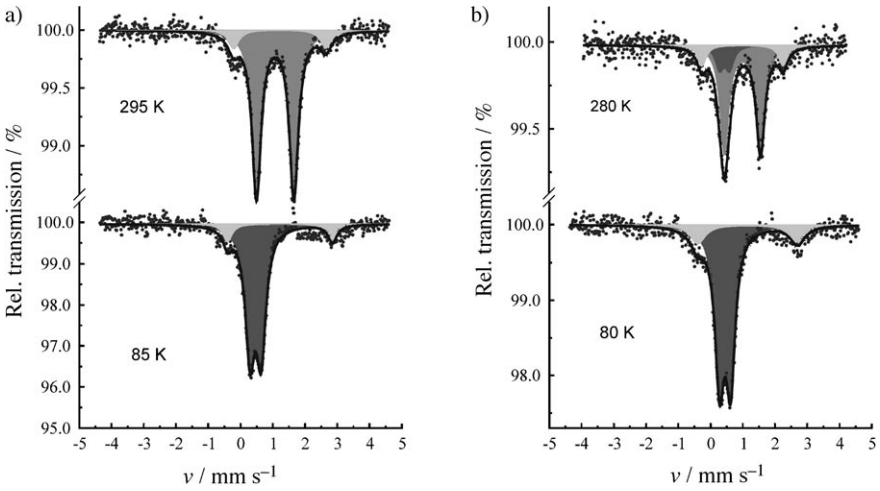

Figure 4. Mössbauer spectra of nanocrystals of **2** (a) and **3** (b) measured at two temperatures. Dark gray: LS; gray and light gray: HS.

The relatively small ΔE_Q value of the HS(1) doublet stems from a large lattice contribution to the electric field gradient (EFG) arising from a distorted (elongated) {FeN_6} core with D_{4h} symmetry, which opposes the valence electron contribution to the EFG. In this case, the xz and yz orbitals are energetically lowest and accommodate, on average, 1.5 electrons per orbital. This gives rise to an EFG contribution which is only one half that of an octahedrally compressed {FeN_6} core, where the xy orbital is lowest and doubly occupied. The origin of the HS(2) doublet may be twofold. First of all, this fraction could reflect the Fe^{II} ions located at the edge of the nanocrystals. It is very likely, particularly in the case of small particles with high specific surface areas, that these Fe^{II} ions "feel" considerable differences in bond strength or even suffer from coordinative defects and consequently do not exhibit SCO. Taking the average size of nanocrystals of **2** and **3**, and the dimensions of the unit cell of **1**·2H_2O, into account, a simple estimation of the possible number of incomplete {FeN_x} coordination sites lying at the edge of the nanocrystals gives a value of around 4% and 12% residual HS centers for **2** and **3**, respectively. It is sensible to associate these incomplete coordination sites with the HS(2)

doublets as they are characterized by a larger ΔE_Q. Although the experimental HS residual fractions are larger, the tendency shown for the population of HS(2) sites mirrors the experimental observation, namely 9–12% for **2** and 14–17% for **3**. Independently of this surface effect, the presence of defects in the crystal can also contribute to the presence of additional HS and/or LS residual fractions in the low- and high-temperature regions, respectively. This fact could account for the 14% of residual LS species trapped in **3** at room temperature.

The cooperativity changes when the particle size decreases, as reflected by a decrease in the width of the hysteresis loop in the $\chi_M T$ vs T curves (25, 22, and 10 K for **1**–**3**, respectively). The particle size and its distribution determine the characteristic T_c and cooperativity of the spin crossover. This dependence of the hysteresis width on particle size for $[Fe(pz)Pt(CN)_4]$ corresponds very well to the behavior predicted by Monte Carlo simulations for cubic or spherical spin-crossover nanoparticles.[14] However, these simulations predict a minimal dependence of T_c on particle size, which is in contrast to what we observe when moving from **1** to **3**. This discrepancy most likely occurs because only short-range interactions are considered in these simulations,[14] whereas both long- and short-range interactions determine the cooperative spin-crossover behavior in the 3D coordination polymer $[Fe(pz)Pt(CN)_4]$.[6a,d,10]

It is worth stressing that the observed modification of the SCO features (critical temperatures, hysteresis width, and residual HS state sites) with smaller nanocrystal size is reminiscent of the properties described for the isomorphic solid solutions $[Fe_{1-x}M^{II}_x(pz)Pt(CN)_4]$ $(0 \le x \le 1,\ M^{II} = Ni, Co)$[10b] (see the Supporting Information). Dilution with non-SCO Ni^{II} or Co^{II} ions reduces the size of the SCO domains progressively, thereby reducing the cooperativity, shifting T_c downwards, transforming the first-order spin transition into a second-order continuous one, and diminishing the hysteresis loop width until it disappears at $x = 0.60$.

In summary, the preparation of nanocrystals of the singular 3D coordination polymer $[Fe(pz)Pt(CN)_4]$, with preservation of the bulk magnetic, structural, and optical bistability down to a particle size of around 50 nm, in water-in-oil microemulsions has been achieved. These nanocrystals are not covered by surfactant, which may allow them to be used in applications near room temperature, such as sensors that exhibit synergy between SCO and adsorption processes or optically switchable memory.

Experimental Section

1: A solution of $K_2[Pt(CN)_4]\cdot 3H_2O$ (43.1 mg, 0.1 mmol) in 2 mL of water was added to a solution of $Fe(BF_4)_2\cdot 6H_2O$ (33.7 mg, 0.1 mmol) and pyrazine (32 mg, 0.4 mmol) in 2 mL of water at a rate of 2 mL h^{-1}. The resulting precipitate was separated by centrifugation, washed with ethanol (96%), and dried in air at ambient temperature. The product formed (**1**·H_2O) was dehydrated at 413 K for 2 h to give **1** as a yellow microcrystalline solid. Yield: 42 mg (97%).

2: A solution of $Fe(BF_4)_2\cdot 6H_2O$ (33.7 mg, 0.1 mmol) and pyrazine (32 mg, 0.4 mmol) in 2 mL of water was added carefully to a solution of NaAOT (9.87 g, 22.2 mmol) in 44 mL of octane and the mixture stirred until formation of a clear water-in-oil microemulsion. The same procedure was applied to $K_2[Pt(CN)_4]\cdot 3H_2O$ (43.1 g, 0.1 mmol) in 2 mL of water to yield a second slightly opaque microemulsion after stirring for 15 min. The two microemulsions were quickly combined and stirred for two days. The precipitate formed was then separated by centrifugation, washed three times with ethanol, and dried in air at ambient temperature to yield **2**·H_2O. This compound was dried at 413 K for 2 h to yield 25 mg (57%) of **2** as an orange-yellow solid in the form of a coalesced fine powder (average dimensions: $230 \times 230 \times 55$ nm^3).

3: The compound **3**·$2.5H_2O$ was synthesized following the same protocol used for **2**·H_2O, but with 67.4 mg of $Fe(BF_4)_2\cdot 6H_2O$, 64 mg of pyrazine, and 86.2 mg of $K_2[Pt(CN)_4]$. Compound **3** (average dimensions: $61 \times 61 \times 21$ nm^3) was obtained as a yellow-orange solid by dehydration of **3**·$2.5H_2O$ at 413 K for 2 h. Yield: 75 mg (86%).

Variable-temperature magnetic susceptibility measurements of all samples (20–30 mg) were performed with a Quantum Design MPMS2 SQUID susceptometer equipped with a 5.5-T magnet operating at 1 T in the temperature interval 1.8–400 K. The susceptometer was calibrated with $(NH_4)_2Mn(SO_4)_2\cdot 12H_2O$. Experimental susceptibilities were corrected for diamagnetism of the constituent atoms using Pascal's constants. Mössbauer spectra were recorded in transmission geometry with a ^{57}Co/Rh source kept at room temperature and a conventional spectrometer operating in the constant-acceleration mode. The samples were sealed in Plexiglass sample holders and mounted in a nitrogen-bath cryostat. The Recoil 1.03a Mössbauer Analysis Software (Dr. E. Lagarec; http://www.isapps.ca/recoil/) was used to fit the experimental spectra. A Seifert XRD 3003 TT diffractometer, with Bragg–Brentano geometry and a Cu tube working at 40 kV and 40 mA with a Ni filter (0.3-mm primary slit, 0.3 mm secondary slit, 0.2 mm detector slit, and scintillation detector), was used for XRPD characterization of the nanocrystals. TEM analysis was performed with a JEOL microscope (JEM-1010; 100 kV) equipped with a MegaView III camera. The "AnalySIS" software was used for image processing. SEM was performed with a Hitachi S-4100 microscope. AFM analysis was performed with a Multimode Scanning Probe Microscope operating in air at room temperature. IR spectra were recorded at 293 K in KBr witha Nicolet 5700 FTIR spectrometer. TGA measurements were performed with a Mettler Toledo TGA/SDTA 851e in the temperature range 300–700 K under nitrogen at a heating rate of 10 K min^{-1}.

Received: April 9, 2008
Published online: July 11, 2008

Keywords: bistability · micelles · nanostructures · spin crossover · thermochromism

[1] a) M. D. Hollingsworth, *Science* **2002**, *295*, 2410–2413; b) C. Janiak, *Dalton Trans.* **2003**, 2781–2804; c) S. Kitagawa, R. Kitaura, S. Noro, *Angew. Chem.* **2004**, *116*, 2388–2430; *Angew. Chem. Int. Ed.* **2004**, *43*, 2334–2375; d) D. Maspoch, D. Ruiz-Molina, J. Veciana, *Chem. Soc. Rev.* **2007**, *36*, 770–818.

[2] a) G. A. Ozin, A. C. Arsenault, *Nanochemistry: A Chemical Approach to Nanomaterials*, The Royal Society of Chemistry, Cambridge, **2005**; b) C. Burda, X. Chen, R. Narayanan, M. A. El-Sayed, *Chem. Rev.* **2005**, *105*, 1025–1102.

[3] a) S. Vaucher, M. Li, S. Mann. *Angew. Chem.* **2000**, *112, 1863–1866; Angew. Chem. Int. Ed.* **2000**, 39, 1793–1796; *Angew. Chem. Int. Ed.* **2000**, *39*, 1793–1796; b) S. Vaucher, J. Fielden, M. Li, E. Dujardin, S. Mann, *Nano Lett.* **2002**, *2*, 225–230; c) T. Uemura, S. Kitagawa, *J. Am. Chem. Soc.* **2003**, *125*, 7814–7815; d) J. M. Domínguez-Vera, E. Colacio, *Inorg. Chem.* **2003**, *42*, 6983–6985; e) L. Catala, T. Gacoin, J. P. Boilot, E. Rivière, C. Paulsen, E. Lhotel, T. Mallah, *Adv. Mater.* **2003**, *15*, 826–829; f) J. G. Moore, E. J. Lochner, C. Ramsey, N. S. Dalal, A. E.

Stiegman, *Angew. Chem.* **2003**, *115*, 2847 – 2849; *Angew. Chem. Int. Ed.* **2003**, *42*, 2741 – 2743.
[4] a) G. Clavel, Y. Guari, J. Larionova, C. Guérin, *New J. Chem.* **2005**, *29*, 275 – 279; b) L. Catala, C. Mathonière, A. Gloter, O. Stephan, T. Gacoin, J. P. Boilot, T. Mallah, *Chem. Commun.* **2005**, 746 – 748; c) L. Catala, A. Gloter, O. Stephan, G. Rogez, T. Mallah, *Chem. Commun.* **2006**, 1018 – 1020; d) G. Clavel, J. Larionova, Y. Guari, C. Guérin, *Chem. Eur. J.* **2006**, *12*, 3798 – 3804.
[5] a) I. Imaz, D. Maspoch, C. Rodríguez-Blanco, J. M. Pérez-Falcón, J. Campo, D. Ruiz-Molina, *Angew. Chem.* **2008**, *120*, 1883 – 1886; *Angew. Chem. Int. Ed.* **2008**, *47*, 1857 – 1860; b) S. Jung, M. Oh, *Angew. Chem.* **2008**, *120*, 2079 – 2081; *Angew. Chem. Int. Ed.* **2008**, *47*, 2049 – 2051.
[6] a) *Spin Crossover in Transition Metal Compounds* (Eds.: P. Gütlich, H. A. Goodwin), *Top. Curr. Chem.* **2004**, *233*, *234*, *235*; b) J. A. Real, A. B. Gaspar, M. C. Muñoz, *Dalton Trans.* **2005**, 2062 – 2079; c) A. B. Gaspar, V. Ksenofontov, M. Seredyuk, P. Gütlich, *Coord. Chem. Rev.* **2005**, *249*, 2661 – 2676; d) J. A. Real, A. B. Gaspar, V. Niel, M. C. Muñoz, *Coord. Chem. Rev.* **2003**, *236*, 121 – 141; e) P. Gütlich, A. Hauser, H. Spiering, *Angew. Chem.* **1994**, *106*, 2109 – 2141; *Angew. Chem. Int. Ed. Engl.* **1994**, *33*, 2024 – 2054.
[7] a) S. Decurtins, P. Gütlich, C. P. Köhler, H. Spiering, A. Hauser, *Chem. Phys. Lett.* **1984**, *105*, 1 – 4; b) A. Hauser, *Top. Curr. Chem.* **2004**, *234*, 155 – 198.
[8] a) N. Ould Moussa, G. Molnár, S. Bonhommeau, A. Zwick, S. Mouri, K. Tanaka, J. A. Real, A. Bousseksou, *Phys. Rev. Lett.* **2005**, *94*, 107205; b) N. Ould Moussa, E. Trzop, S. Mouri, S. Zein, G. Molnár, A. B. Gaspar, E. Collet, M. Buron, J. A. Real, S. Borshch, K. Tanaka, H. Cailleau, A. Bousseksou, *Phys. Rev. B* **2007**, *75*, 054101; c) E. Trzop, M. Buron-Le Cointe, H. Cailleau, L. Toupet, G. Molnár, A. Bousseksou, A. B. Gaspar, J. A. Real, E. Collet, *J. Appl. Crystallogr.* **2007**, *40*, 158 – 164.
[9] a) A. Galet, A. B. Gaspar, M. C. Muñoz, G. V. Bukin, G. Levchenko, J. A. Real, *Adv. Mater.* **2005**, *17*, 2949 – 2953; b) O. Kahn, C. J. Martinez, *Science* **1998**, *279*, 44 – 48; c) O. Kahn, J. Kröber, C. Jay, *Adv. Mater.* **1992**, *4*, 718 – 728.
[10] a) V. Niel, J. M. Martinez-Agudo, M. C. Muñoz, A. B. Gaspar, J. A. Real, *Inorg. Chem.* **2001**, *40*, 3838 – 3839; b) T. Tayagaki, A. Galet, G. Molnár, M. C. Muñoz, A. Zwick, K. Tanaka, J. A. Real, L. Dubrovinsky, A. Bousseksou, *J. Phys. Chem. B* **2005**, *109*, 14859 – 14867.
[11] a) S. Cobo, G. Molnár, J. A. Real, A. Bousseksou, *Angew. Chem.* **2006**, *118*, 5918 – 5921; *Angew. Chem. Int. Ed.* **2006**, *45*, 5786 – 5789; b) G. Molnár, S. Cobo, J. A. Real, F. Carcenac, E. Daran, C. Vieu, A. Bousseksou, *Adv. Mater.* **2007**, *19*, 2163 – 2167; c) S. Bonhommeau, G. Molnár, A. Galet, A. Zwick, J. A. Real, J. J. McGarvey, A. Bousseksou, *Angew. Chem.* **2005**, *117*, 4137 – 4141; *Angew. Chem. Int. Ed.* **2005**, *44*, 4069 – 4073.
[12] a) E. Coronado, J. R. Galán-Mascarós, M. Monrabal-Capilla, J. García-Martínez, P. Pardo-Ibañez, *Adv. Mater.* **2007**, *19*, 1359 – 1361; b) O. Fouché, J. Degert, N. Daro, T. Forestier, C. Deplanche, J. F. Lètard, E. Freysz, presented at the European Conference on Molecular Magnetism, Tomar, Portugal, October **2006**; c) J. F. Lètard, Nguyen, N. Daro, in French, PCT Intl Appl, WO 2007065996, **2007**, 31 pp, CODEN: PIXXD2.
[13] J. Eastoe, M. J. Hollamby, L. Hudson, *Adv. Colloid Interface Sci.* **2006**, *128/130*, 5 – 15.
[14] T. Kawamoto, S. Abe, *Chem. Commun.* **2005**, 3933 – 3933.

